Atomic hydrogen passivation for photoresponsivity enhancement of boron-doped p-BaSi$_2$ films and performance improvement of boron-doped p-BaSi$_2$/n-Si heterojunction solar cells

Zhihao Xu, Takuma Sato, iD Louise Benincasa, et al.

View Online   Export Citation   CrossMark

ARTICLES YOU MAY BE INTERESTED IN

p-BaSi$_2$/n-Si heterojunction solar cells with conversion efficiency reaching 9.0%
Applied Physics Letters **108**, 152101 (2016); https://doi.org/10.1063/1.4945725

Effect of amorphous Si capping layer on the hole transport properties of BaSi$_2$ and improved conversion efficiency approaching 10% in p-BaSi$_2$/n-Si solar cells
Applied Physics Letters **109**, 072103 (2016); https://doi.org/10.1063/1.4961309

Point defects in BaSi$_2$ thin films for photovoltaic applications studied by positron annihilation spectroscopy
Journal of Applied Physics **127**, 085304 (2020); https://doi.org/10.1063/1.5126264

Atomic hydrogen passivation for photoresponsivity enhancement of boron-doped p-BaSi₂ films and performance improvement of boron-doped p-BaSi₂/n-Si heterojunction solar cells

Zhihao Xu,[1] Takuma Sato,[1,2] Louise Benincasa,[1,3] (ID) Yudai Yamashita,[1] Tianguo Deng,[1] Kazuhiro Gotoh,[4] (ID)
Kaoru Toko,[1] (ID) Noritaka Usami,[4] (ID) Andrew B. Filonov,[5] Dmitri B. Migas,[5,6] Denis A. Shohonov,[7]
and Takashi Suemasu[1,a] (ID)

AFFILIATIONS

[1]Institute of Applied Physics, University of Tsukuba, Tsukuba, Ibaraki 305-8573, Japan
[2]Inorganic and Biological Chemistry Department, Université Grenoble Alpes, CEA, CNRS, IRIG, SyMMES, 38000 Grenoble, France
[3]Materials Department, University of Grenoble-Alpes, 38400 Saint-Martin-d'Heres, France
[4]Graduate School of Engineering, Nagoya University, Nagoya 464-8603, Japan
[5]Department of Micro- and Nanoelectronics, Belarusian State University of Informatics and Radioelectronics, P. Brovki 6,
220013 Minsk, Belarus
[6]Moscow Engineering Physics Institute, National Research Nuclear University, Kashirskoe Shosse 31, 115409 Moscow, Russia
[7]Institute of Applied Physics, National Academy of Sciences of Belarus, Academicheskaya 16, 220072 Minsk, Belarus

[a]Author to whom correspondence should be addressed: suemasu.takashi.gu@u.tsukuba.ac.jp

ABSTRACT

Semiconducting barium disilicide (BaSi₂) is an emerging material for solar cell applications, and therefore, defect passivation is critical for improving its solar cell performance. Herein, the effect of atomic hydrogen (H) on the photoresponsivity of 500 nm-thick boron (B)-doped p-BaSi₂ films was examined. The photoresponsivity reached ∼4 A/W (about twice the highest reported value for H-passivated undoped BaSi₂ films) in B-doped p-BaSi₂ films exposed to an atomic H supply for $5-10$ min because of an increased minority-carrier lifetime, as measured by the microwave-detected photoconductivity decay. Furthermore, a ≥ 15 min atomic H supply was found to degrade photoresponsivity. *Ab initio* studies were used to interpret and understand experimental observations by analyzing states in the gap region, which can act as traps, in B-doped p-BaSi₂ with H incorporation. The effect that atomic H had on the performance of B-doped p-BaSi₂/n-Si heterojunction solar cells was also studied. The saturation current density was found to decrease by three orders of magnitude with the atomic H supply, and the conversion efficiency was increased up to 6.2%. Deep-level transient spectroscopy revealed a reduction of defect densities induced by the atomic H supply. Both experimental and theoretical viewpoints show that an atomic H supply is beneficial for BaSi₂ solar cells.

I. INTRODUCTION

Thin-film solar cell materials such as Cu(In,Ga)Se₂ and CdTe have been studied extensively[1–5] owing to their high efficiencies (η) above 22%.[6] In addition, GaAs has received renewed interest since the 2019 report of an ∼0.2 μm-thick GaAs solar cell with a certified η of 19.9% using a nanostructured silver back mirror.[7] Perovskite solar cells are also currently the center of investigation,[8,9] but these materials comprise toxic or scarce elements. Considering these circumstances, we have focused on semiconducting barium disilicide (BaSi₂).[10,11] BaSi₂ has attractive features such as a suitable bandgap ($E_g = 1.3$ eV) for a single-junction solar cell, high absorption coefficients (α) exceeding those of Cu(In,Ga)Se₂,[12–15] a long minority-carrier lifetime (τ) above 10 μs,[16,17] and a large minority-carrier

diffusion length ($L \approx 10\,\mu$m) owing to inactive grain boundaries.[18] Recently, with the help of amorphous Si (a-Si) passivation layers,[19] we achieved an η approaching 10% in p-BaSi$_2$/n-Si heterojunction solar cells[20] and demonstrated the operation of BaSi$_2$ homojunction solar cells.[21] We are now focusing on further improvement of the optical and transport properties of BaSi$_2$ films. According to a first-principles calculation,[22] from the viewpoint of formation energy, Si vacancies (V_{Si}) are most likely to occur among point defects in BaSi$_2$. The presence of defects in BaSi$_2$ films and bulk polycrystalline BaSi$_2$ has been measured by deep-level transient spectroscopy (DLTS),[23] Raman spectroscopy,[24] electron paramagnetic resonance,[25] and photoluminescence (PL).[26] The measured PL spectrum of bulk BaSi$_2$ is reproduced well by four curves with peaks located at P1 (0.83 eV), P2 (0.95 eV), P3 (1.03 eV), and P4 (1.12 eV), showing the presence of defect states within the bandgap.[26] Therefore, passivation of defects in BaSi$_2$ films is critical for their use in solar cell applications such as crystalline Si solar cells. Our previous research has shown that defects in undoped BaSi$_2$ films are passivated by atomic hydrogen (H).[27] Specifically, the photoresponsivity of undoped BaSi$_2$ films is markedly enhanced by supplying atomic H after the growth of BaSi$_2$ films for 15 min owing to the improved carrier lifetime, as measured via microwave-detected photoconductivity decay (μ-PCD).[27] The basic structure of this solar cell is a p–n junction; thus, passivation of impurity-doped p- or n-BaSi$_2$ films is of particular importance as a next step.

In this paper, we first investigate the effect of atomic H passivation on the photoresponse properties of lightly and heavily B-doped p-BaSi$_2$ films both experimentally and theoretically. These films were selected because they are used as the light absorbing layer and emitting layer in solar cells, respectively. Recent experiments have shown that lightly B-doped p-BaSi$_2$ films are more promising as a light absorbing layer than undoped ones.[28] We next discuss the effect of atomic H on the performance of p-BaSi$_2$/n-Si solar cells.

II. METHODS

A. Formation of atomic hydrogen-passivated p-BaSi$_2$ and p-BaSi$_2$/n-Si solar cells

Fabrication and subsequent H passivation of B-doped BaSi$_2$ films were accomplished using an ion-pumped molecular beam epitaxy system equipped with standard Knudsen cells (K-cells) for Ba and B, an electron-beam gun for Si, and a radio-frequency plasma generator for atomic H. First, Ba, Si, and B atoms were co-deposited on a low-resistivity ($\rho = 0.01\,\Omega$ cm) Czochralski-grown (CZ) n$^+$-Si(111) substrate at a substrate temperature of $T_S = 600\,$°C to form an approximately 500 nm-thick B-doped BaSi$_2$ thin film. The crucible temperature of the B K-cell was set at $T_B = 1100$ or $1230\,$°C for light or heavy B doping, respectively, wherein the respective hole concentrations were $p = 7 \times 10^{16}$ or 3×10^{18} cm^{-3} at room temperature (RT). Hereafter, we refer to these as "lightly B-doped" and "heavily B-doped" samples, respectively. Second, the atomic H was supplied to the samples via a plasma generator for varying durations ($t_{BaSi:H}$) at $T_S = 600\,$°C. During an atomic H supply, the vacuum level was maintained at 10^{-3} Pa, the plasma power was set at 10 W, and the H concentration was $\sim 10^{19}$ cm^{-3}.[27] Finally, 3 nm-thick a-Si was deposited as a capping layer.[18] The samples grown on the low-ρ Si substrates were used for photoresponsivity

TABLE I. Structure, substrate growth temperature (T_S), H supply duration ($t_{BaSi:H}$), and B crucible temperature (T_B) for the samples grown herein.

Structure	Sample	T_S (°C)	$t_{BaSi:H}$ (min)	T_B (°C)
a-Si/B-doped p-BaSi$_2$:H	Reference	580	15	0
(500 nm)/n$^+$-Si($\rho = 0.01\,\Omega$ cm)	1	600	0	1100
	2		5	
	3		10	
	4		15	
	5		0	1230
	6		1	
	7		5	
a-Si/B-doped p-BaSi$_2$:H	8	600	0	1100
(500 nm)/n-Si($\rho > 1000\,\Omega$ cm)	9		5	
	10		10	

measurements. Samples were also grown under the same conditions on a high-ρ ($> 1000\,\Omega$ cm) floating-zone (FZ) n-Si(111) substrate for μ-PCD measurements and Hall measurements by the van der Pauw method at RT. Sample preparation details are summarized in Table I. To study the effect of H passivation on the performance of B-doped p-BaSi$_2$/n-Si heterojunction solar cells, we formed 20 nm-thick B-doped p-BaSi$_2$ layers on n-Si(111) substrates ($\rho = 1$–$4\,\Omega$ cm) at $T_S = 600\,$°C and $T_B = 1230\,$°C. Then, atomic H was supplied for $t_{BaSi:H} = 14$ or 32 s, followed by a 3 nm-thick a-Si capping layer. Sample preparation details are summarized in Table II.

For measurements of the photoresponse and the current density vs voltage (J–V) curves under AM1.5 illumination, 80 nm-thick indium tin oxide (ITO) electrodes (1 mm diameter) were fabricated on the front surface of the samples and 150 nm-thick Al was deposited on the back surface of the samples. Photoresponse spectra were measured by a lock-in technique using a xenon lamp (Bunko Keiki, SM-1700A, Japan) and a single monochromator with a focal length of 25 cm (Bunko Keiki, RU-60N, Japan). The light intensity of the lamp was calibrated using a pyro-electric sensor (Melles Griot, 13PEM001/J). The photoconduction was used to measure the photoresponsivity of BaSi$_2$ films. A bias voltage of 0.3 V was applied to the front ITO electrode with respect to the Al electrode to extract photogenerated electrons at the front ITO electrode. This represents a "forward" bias voltage for the p-BaSi$_2$/n-Si diodes. While such forward bias voltages to pn diodes usually reduce photoresponsivity, there was no difference between both the forward and reverse bias voltages in this work because the

TABLE II. Structure, substrate growth temperature (T_S), H supply duration ($t_{BaSi:H}$), and B crucible temperature (T_B) for the p-BaSi$_2$/n-Si solar cells.

Structure	Sample	T_S (°C)	$t_{BaSi:H}$ (s)	T_B (°C)
a-Si/B-doped p-BaSi$_2$:H	11	600	0	1230
(20 nm)/n-Si($\rho = 1$–$4\,\Omega$ cm)	12		14	
	13		30	

diodes did not display rectifying properties according to the J–V characteristics. The PL measurements were carried out at 8 K with an excitation laser wavelength of 442 nm and detected by a liquid nitrogen-cooled InP/InGaAs photomultiplier (Hamamatsu Photonics R5509-72, Japan) and amplified by the lock-in technique. Samples were excited from the $BaSi_2$ side. The carrier lifetime τ was measured using a μ-PCD system (Kobelco, LTA-1512EP, Japan), while the DLTS measurement was carried out in the temperature range of 80–300 K using a 1 MHz capacitance vs voltage (C–V) meter (HP 4280A). The rate window was varied between 1 and 512 ms.

B. Computational details

To estimate the influence of B doping and H incorporation on the electronic properties of $BaSi_2$, the first-principles total energy projector-augmented wave method (VASP code)[29–31] was used, which was also used for full structural optimization (i.e., lattice parameters and atomic positions). Because one crystallographic unit cell of $BaSi_2$ (space group $Pnma$, $a = 8.942$ Å, $b = 6.733$ Å, and $c = 11.555$ Å with Ba(1)–Ba(2) and Si(3)–Si(5) chemically inequivalent sites)[32] is not sufficiently large to avoid strong defect–defect interactions, we used an enlarged $2 \times 3 \times 2$ unit cell (see Fig. 1). A similar approach was previously used by us for $BaSi_2$ containing V_{Si} with and without H incorporation,[27] doped by O[33] and H.[34] For the exchange and correlation potentials, the generalized gradient approximation of Perdew–Burke–Ernzerhof[35] has been implemented. The energy cutoff of 400 eV and a $5 \times 5 \times 5$ mesh of Monkhorst–Pack points for the Brillouin zone integration were sufficient to ensure total energy convergence. A criterion of 0.05 eV/Å for the force acting on the atoms was chosen to stop structural relaxation. The total density of states (DOS) was calculated using the tetrahedron method with Blöchl corrections, which excludes any smearing techniques.
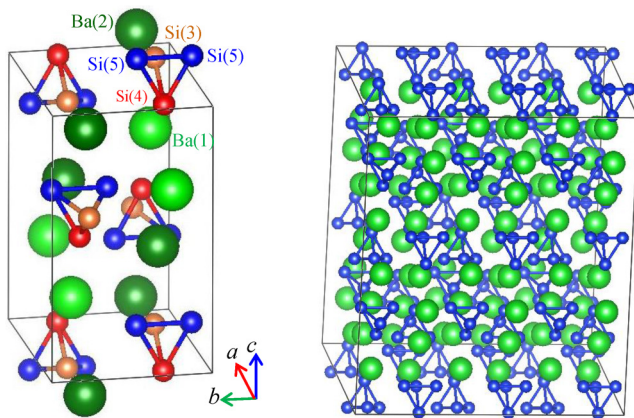
III. RESULTS AND DISCUSSIONS

A. Effect of atomic H on lightly B-doped and heavily B-doped p-$BaSi_2$ films

Figure 2(a) shows the photoresponse spectra of lightly B-doped p-$BaSi_2$ films from samples 1–4, where $t_{BaSi:H}$ was varied in the range

(a)

(b)
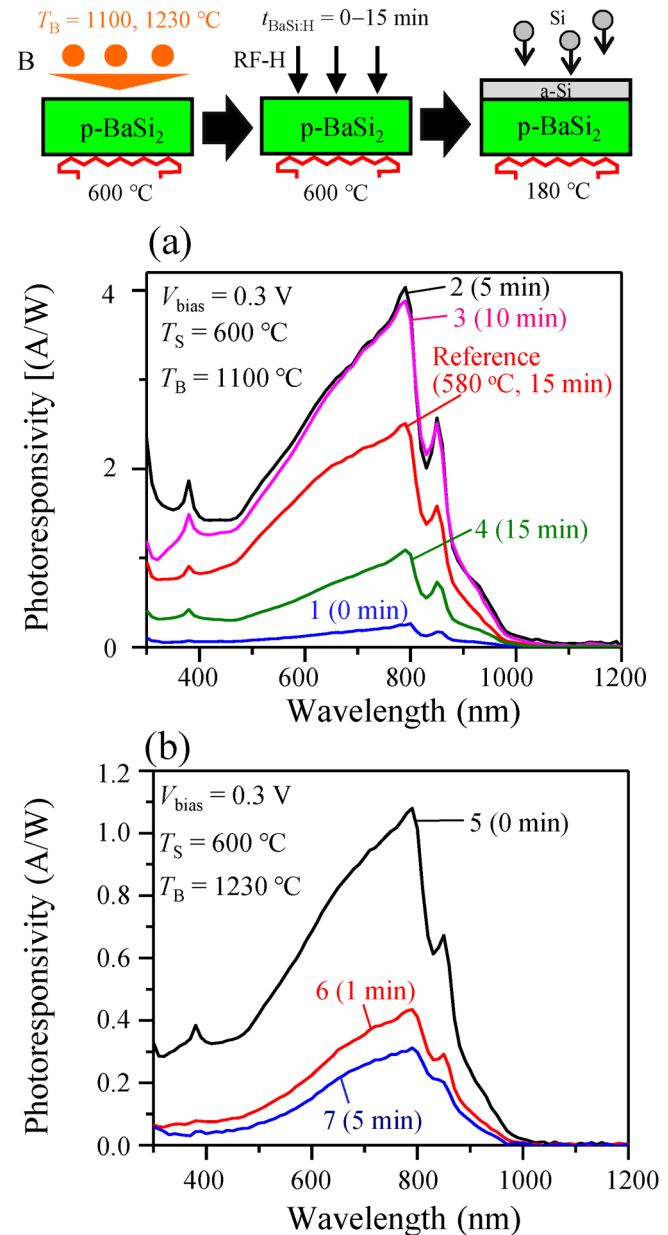
FIG. 2. Photoresponse spectra of 500 nm-thick (a) lightly B-doped $BaSi_2$ layers passivated by atomic H with various values of $t_{BaSi:H}$ in the range of 0−15 min; and (b) heavily B-doped $BaSi_2$ layer passivated by atomic H with various values of $t_{BaSi:H}$ in the range of 0−5 min.

FIG. 1. Crystal structure of orthorhombic $BaSi_2$: (left panel) one crystallographic unit cell, possessing two inequivalent Ba sites Ba(1) and Ba(2) and three inequivalent Si sites Si(3)–Si(5); (right panel) the $2 \times 3 \times 2$ enlarged unit cell used for calculations.

of 0−15 min. As a reference, we included the spectrum of the highest photoresponsivity of undoped BaSi$_2$ films ($t_{BaSi:H}$ = 15 min).[27] The photoresponsivity increased at wavelengths λ < ∼1000 nm, corresponding to E_g of BaSi$_2$. The photoresponsivity is proportional to the ratio of the carrier lifetime to the carrier transit time for both radiative and non-radiative photogenerated carrier recombination.[36] Hence, it is influenced by the density of active defects. The smallest photoresponsivity was obtained for sample 1, which was prepared without H passivation. The photoresponsivity of samples 2 ($t_{BaSi:H}$ = 5 min) and 3 ($t_{BaSi:H}$ = 10 min) increased significantly more than that of sample 1, reaching a maximum value of ∼4 A/W at λ = 800 nm. This is almost twice the highest value previously reported for H-passivated undoped BaSi$_2$ films (reference sample, $t_{BaSi:H}$ = 15 min). Comparing the photoresponse spectrum of sample 3 to that of sample 2, the photoresponsivity of sample 3 was smaller at shorter wavelengths (i.e., λ < 500 nm). This behavior is interpreted to originate from the surface damage induced by atomic H. We posit that the energetic H atoms from the plasma generator that hit the sample surface generated defects in the surface regions. These defects caused the photogenerated electrons to be more likely to recombine before being extracted to the ITO electrodes. The photoresponsivity of sample 4 ($t_{BaSi:H}$ = 15 min) exhibited further degradation, signifying that both the bulk and surface regions acquired defects. In the bulk region, the superabundant H atoms generated additional defects other than V_{Si}, and the same phenomenon was previously observed in crystalline Si (c-Si).[37]

Figure 2(b) shows the photoresponse spectra of heavily B-doped p-BaSi$_2$ films from samples 5–7, where $t_{BaSi:H}$ was varied in the range of 0−5 min. In contrast with samples 1–4, the photoresponsivity exhibited degradation with increasing $t_{BaSi:H}$, showing that H passivation is not suitable to improve the photoresponsivity of heavily B-doped p-BaSi$_2$ films. Note that the photoresponsivity of heavily B-doped BaSi$_2$ films in sample 5 ($t_{BaSi:H}$ = 0 min) is higher than lightly B-doped BaSi$_2$ films in sample 1 ($t_{BaSi:H}$ = 0 min), meaning that the lightly B-doped BaSi$_2$ films contain more defects than heavily B-doped ones.

We investigated the PL of the H-passivated lightly and heavily B-doped p-BaSi$_2$ films to explain the effects of H passivation and understand the localized states related to radiative recombination. The PL intensity is proportional to the ratio of the radiative recombination rate of photogenerated carriers to their total recombination rate. The PL offers a nondestructive and sensitive tool for defect studies in solar cell materials such as Si,[38–40] Cu(In,Ga)Se$_2$,[41–43] III–V semiconductors,[44,45] CdTe,[46,47] and perovskites,[48] and they provide information on the presence of localized states within the bandgap. The PL spectra were measured at 8 K for lightly B-doped p-BaSi$_2$ films from samples 1 ($t_{BaSi:H}$ = 0 min), 2 ($t_{BaSi:H}$ = 5 min), and 4 ($t_{BaSi:H}$ = 15 min), as shown in Figs. 3(a)−3(c), respectively. The results for heavily B-doped p-BaSi$_2$ films from samples 5 ($t_{BaSi:H}$ = 0 min) and 7 ($t_{BaSi:H}$ = 5 min) are in Figs. 3(d) and 3(e), respectively. As shown in Figs. 3(a) and 3(d), without H treatment, the lightly B-doped sample (sample 1) had a much smaller PL intensity than the heavily B-doped one (sample 5), which shows that the nonradiative recombination rate due to defects is much higher in sample 1 than in sample 5. Because B atoms are expected to fill V_{Si} in BaSi$_2$ films, more V_{Si} might be passivated in

sample 5 because the p-BaSi$_2$ films contained more B atoms than in sample 1. We expect that this is the reason for higher PL intensity and photoresponsivity in sample 5 compared with sample 1. In samples 2 and 4, the measured spectra were reproduced by three Gaussian curves with peaks located at P2, P3, and P4. In sample 4, the contribution of P2, which is associated with levels deeper than for those in P3 and P4, becomes dominant. From the viewpoint of the Shockley–Read–Hall recombination model,[49] deeper levels such as these promote the recombination of photogenerated carriers. In this regard, the degradation of photoresponsivity in sample 4 compared with sample 2 is consistent with the PL results. Figures 3(d) and 3(e) show the PL spectra of heavily B-doped p-BaSi$_2$ films in sample 5 ($t_{BaSi:H}$ = 0 min) and sample 7 ($t_{BaSi:H}$ = 5 min), respectively. We note that P1, which is associated with deeper levels, is necessary to reproduce the measured PL spectra of sample 5 but not that of sample 7. Considering that deeper levels like P1 in sample 5 promote carrier recombination and thus decrease the photoresponsivity, the disappearance of P1 in sample 7 might increase the photoresponsivity, although this differs from the obtained experimental results in Fig. 2(b). We, therefore, speculate that non-radiative recombination processes, which cannot be detected via PL measurements, occur in the heavily B-doped p-BaSi$_2$ films with increasing $t_{BaSi:H}$.

Figures 4(a) and 4(b) show the RT dependence of p and the hole mobility on $t_{BaSi:H}$ for the lightly and heavily B-doped p-BaSi$_2$ films, respectively. Several reports have been published on the neutralization of shallow acceptor and donor impurity levels on p variation in c-Si by atomic H passivation.[50,51] Therefore, p would also change owing to H passivation in heavily B-doped BaSi$_2$. In Fig. 4(a), p of lightly B-doped p-BaSi$_2$ films was slightly increased from 7×10^{16} to ∼1×10^{17} cm^{-3} when $t_{BaSi:H}$ was lengthened from 0 to 10 min, and the mobility correspondingly decreased from 80 to 75 cm^2 V^{-1} s^{-1}. A similar trend was observed in heavily B-doped p-BaSi$_2$ [Fig. 4(b)], wherein the p value slightly increased from 3×10^{18} to ∼7×10^{18} cm^{-3} when $t_{BaSi:H}$ was lengthened from 0 to 5 min, and the mobility correspondingly decreased from 41 to 23 cm^2 V^{-1} s^{-1}. The variation of p is discussed later in Sec. III B.

B. Photoconductance decay curves

Based on the improvement in the photoresponsivity of the atomic H-passivated lightly B-doped p-BaSi$_2$ films (sample 2) shown in Fig. 2(a), it is reasonable to consider that τ might be improved for this sample. The photoresponsivity is proportional to the ratio of the carrier lifetime to the carrier transit time.[36] Therefore, enhanced photoresponsivity is attributed to an increase in carrier lifetime and/or a decrease in the carrier transit time. In Fig. 4(a), the mobility did not exhibit a large change with increased $t_{BaSi:H}$. Therefore, an increase in carrier lifetime is anticipated. To confirm this, we carried out μ-PCD measurements on samples 8–10, whose growth conditions were the same as those for samples 1–3. For the μ-PCD measurements, high-ρ FZ-Si substrates were used in samples 8–10 instead of low-ρ CZ-Si substrates (in samples 1–3) to suppress the microwave intensity reflected from the Si substrate. Figure 5(a) shows the normalized photoconductance decay curves of samples 8–10 excited by a 5 ns pulsed laser intensity (λ = 349 nm) of 1.3×10^5 W/cm^2. Assuming that the reflectivity of
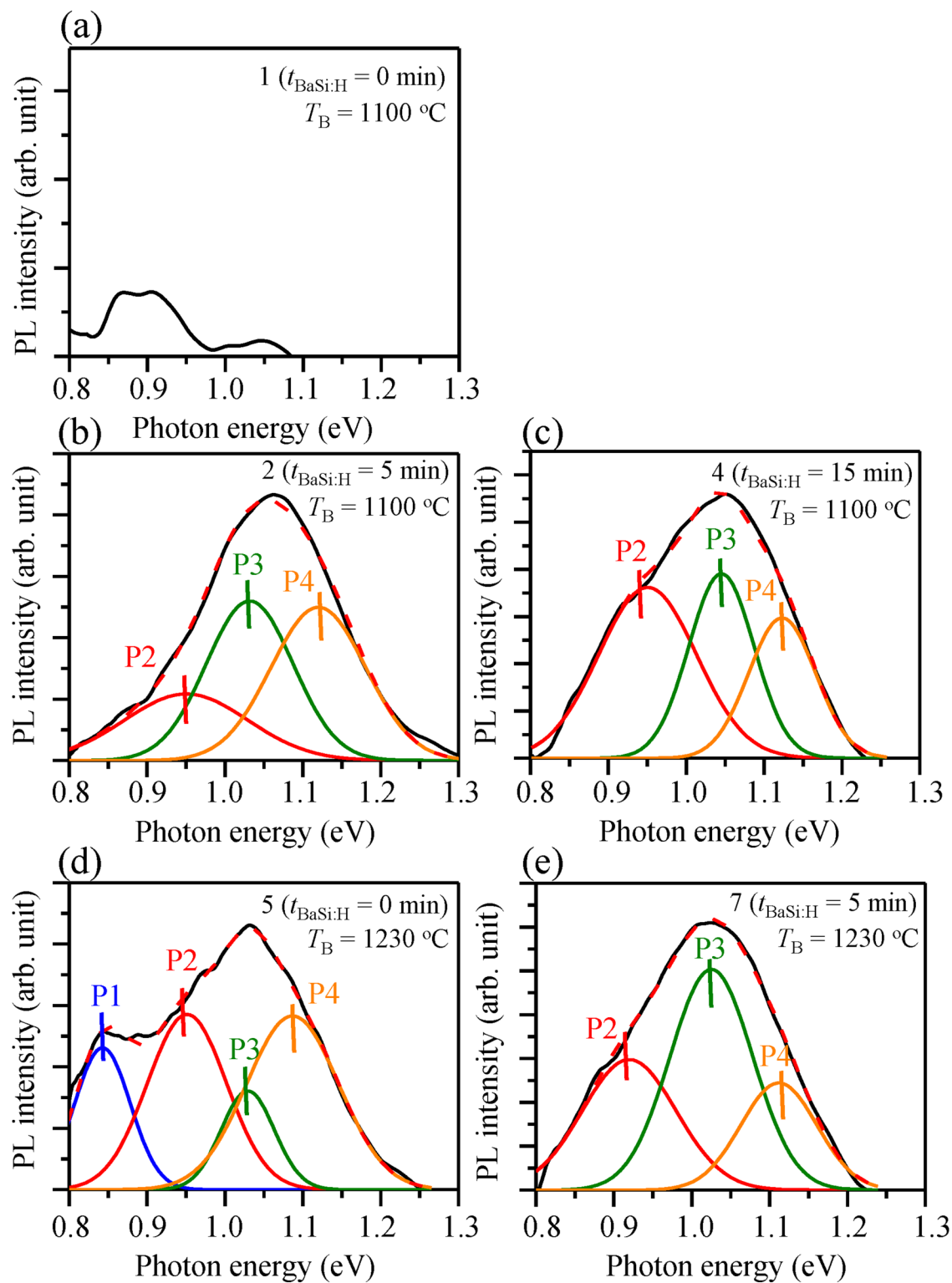
FIG. 3. PL spectra measured at 8 K for samples (a) 1, (b) 2, (c) 4, (d) 5, and (e) 7, fitted using Gaussian curves.
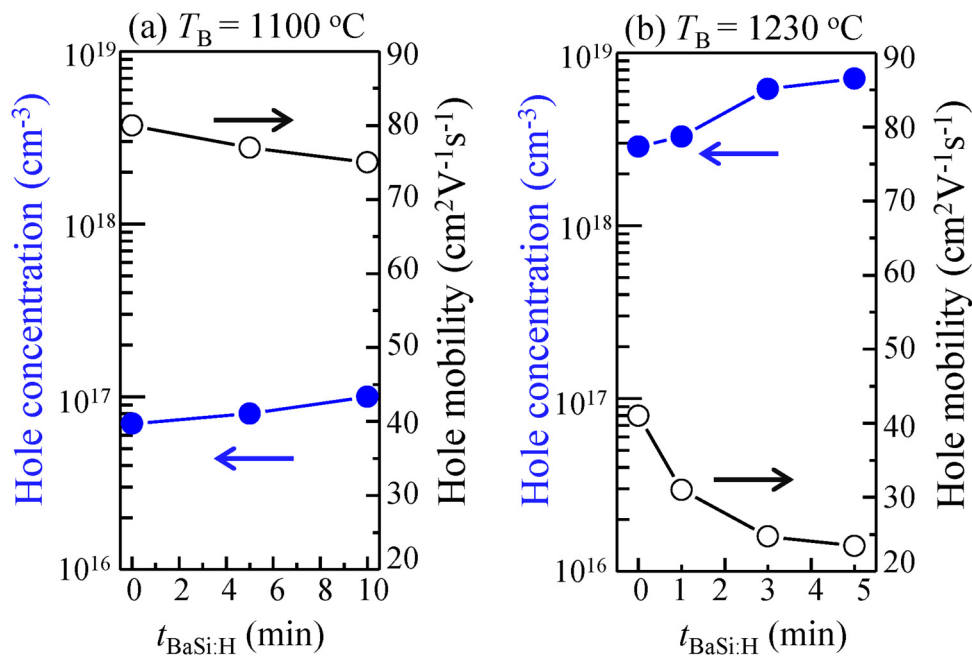
FIG. 4. Carrier concentration (left axis) and mobility (right axis) in the H-passivated (a) lightly B-doped BaSi$_2$ and (b) heavily B-doped BaSi$_2$, as a function of $t_{BaSi:H}$.

microwaves is proportional to the excess carrier concentration, we can deduce the value of τ from the decay curves. Electrons and holes were generated by the 5 ns laser pulse in a spot with a 2 mm diameter. The photoconductance decay was measured from the reflectivity of microwaves with a frequency of 26 GHz. The estimated areal photon density is given by $\Phi = I_{ph}t_{ph}\lambda/(hc)$, where I_{ph} is the laser intensity $(1.3 \times 10^5 \, \text{J}\,\text{s}^{-1}\,\text{cm}^2)$, t_{ph} is the laser pulse duration $(5 \times 10^{-9} \, \text{s})$, λ is the laser wavelength (349 nm), and hc is Plank's constant multiplied by the speed of light $(1.99 \times 10^{-16} \, \text{J}\,\text{nm})$. We find the $\Phi \approx 1.1 \times 10^{15} \, \text{cm}^{-2}$. It was assumed that photogenerated carriers were uniformly distributed over the 500 nm-thick H-passivated lightly B-doped BaSi$_2$. The electron–hole pair concentration is calculated to be $2.2 \times 10^{19} \, \text{cm}^{-3}$ on average, while α at $\lambda = 349$ nm is higher than $5 \times 10^5 \, \text{cm}^{-1}$.[12] Thus, most of the photons at this wavelength are absorbed when they travel approximately 60 nm from the surface. Here, we define $\tau_{1/e}$ as the time when the reflected microwave intensity decreases by $\exp(-1)$ from the initial value after the excitation laser was turned off. In Fig. 5(a), $\tau_{1/e}$ was calculated to be 0.13, 1.20, and 0.40 μs for samples 8, 9, and 10, respectively. The τ of sample 9 is nine times larger than that of sample 8, signifying that the H passivation significantly improves the minority carrier properties. We, therefore, assert that the increase in τ is the reason for the distinct photoresponsivity improvement in samples 2 and 3 in Fig. 2(a). Figure 5(b) shows the photoconductance decay curves of samples 8 and 10, excited by a 5 ns pulsed laser intensity ($\lambda = 909$ nm) of $1.3 \times 10^5 \, \text{W/cm}^2$. Because of the much smaller α, most of the photons at this wavelength are absorbed in the c-Si substrate. The electron concentration in the Si substrate is approximately $n = 10^{13} \, \text{cm}^{-3}$.

Unexpectedly, the τ of the Si substrate, which is governed by carrier recombinations mainly at the BaSi$_2$/Si interface and the Si back surface, improved from 12 μs in sample 8 to 25 μs in sample 10. This provides supporting evidence that atomic H-passivated defects around the BaSi$_2$/Si interface.

We next discuss the improvement of carrier lifetime in lightly B-doped p-BaSi$_2$ films from a theoretical viewpoint. The photoresponsivity and minority-carrier lifetimes of BaSi$_2$ passivated with atomic H have recently been considered,[27] and a model describing these non-radiative processes has been proposed and various trap-related recombination mechanisms have been accounted for. The only "free" parameter of this model was the trap concentration. We applied this approach to simulate the photoconductance decay curve behavior in the lightly B-doped p-BaSi$_2$ films fabricated using different $t_{BaSi:H}$, as shown in Fig. 6. From the best fit of experimental data, the obtained trap concentration was found to be 7.5×10^{14}, 4.5×10^{13}, and $1.5 \times 10^{14} \, \text{cm}^{-3}$ for the samples with $t_{BaSi:H} = 0$, 5, and 10 min, respectively. The more pronounced decrease in photoconductivity for the samples with $t_{BaSi:H} = 0$ and 10 min compared with the sample with $t_{BaSi:H} = 5$ min is caused by the higher trap concentrations. It is interesting to compare the present results with those obtained for the undoped case,[27] where we had qualitatively the same situation for the photoconductance decay curve behavior of the BaSi$_2$ samples with $t_{BaSi:H} = 1$, 15, and 30 min. Furthermore, the values of the trap concentration were 6.5×10^{13}, 2.2×10^{12}, and $2.1 \times 10^{13} \, \text{cm}^{-3}$, respectively, and it was assumed that the trap centers could be associated with Si vacancy complexes. First, it should be noted here that for lightly B-doped BaSi$_2$ films, the appropriate trap concentration values are about
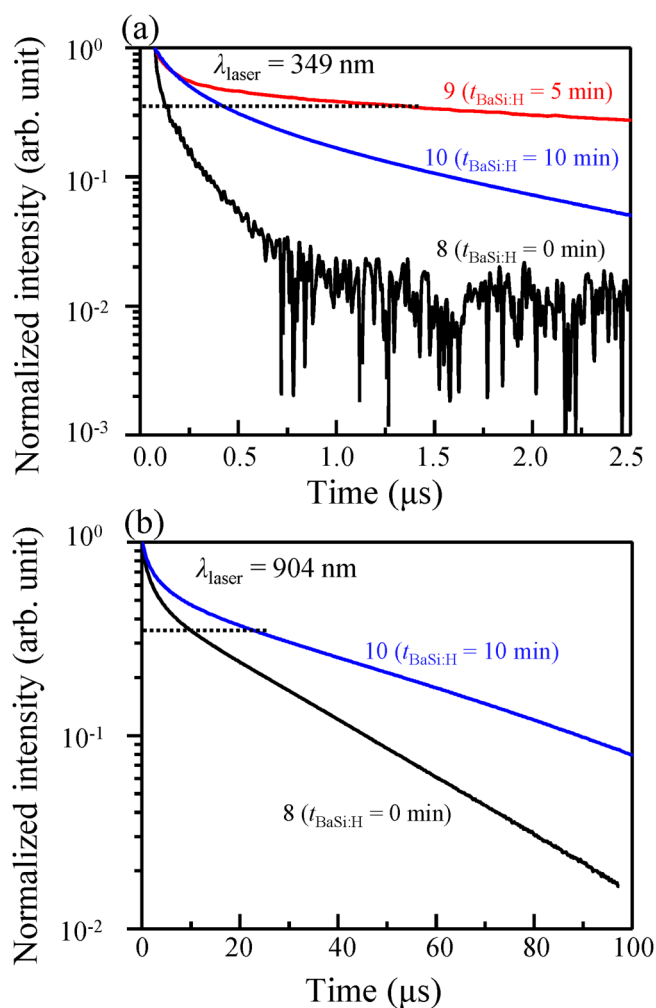
FIG. 5. Photoconductance decay curves of atomic H-passivated lightly B-doped BaSi$_2$ with different $t_{BaSi:H}$ with laser wavelength of (a) 349 and (b) 904 nm.

FIG. 6. Normalized photoconductivity of samples B-doped BaSi$_2$ vs time t after excitation was discontinued. Comparison of experimental data [data points, Fig. 5(a)] with theoretical estimations (solid lines). Photoconductivity is normalized to the value at $t = 0$.

one order of magnitude greater than those for the undoped material. Accounting for the fact that the concentration of the Si vacancy complexes does not exceed a value on the order of 10^{13} cm^{-3} (in the present situation, it should be even less because some B atoms will occupy the empty Si positions), it can be expected that other types of defects will contribute to the high concentration of the trap centers. Analyzing the p-type carrier mobility vs temperature in B-doped BaSi$_2$,[52] it was shown that the presence of a high concentration of neutral defects (mainly interstitial B atoms) is a characteristic feature of the studied samples. Thus, we assume that such B interstitial atoms (and particularly H interstitial atoms as well) are associated with the trap centers in B-doped BaSi$_2$. Second, a remaining question is why the minimal value of the trap concentration (i.e., maximal "passivation" effect) is reached after only 5 min of H-plasma treatment for the B-doped BaSi$_2$, in contrast with the 15 min required for the undoped
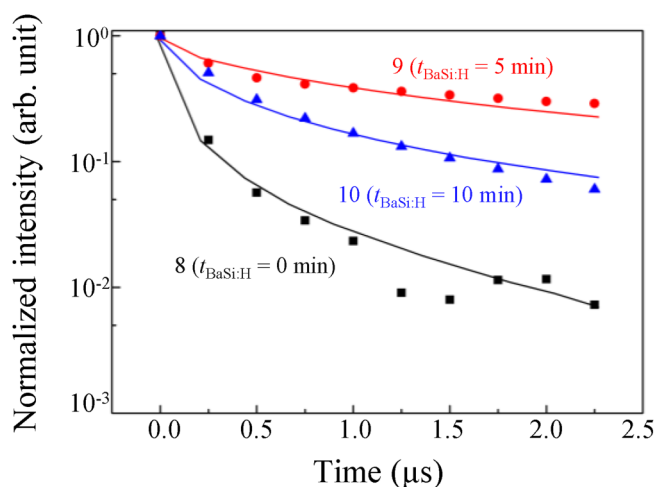
samples. Finally, to reproduce the experimental photoconductance data for the heavily B-doped BaSi$_2$ samples, our estimates gave a trap concentration value of ~10^{15} cm^{-3} or greater.

To get more insight into the defect levels with and without H treatment, we next performed *ab initio* modeling of various B-doped BaSi$_2$ structures with possible incorporated H atoms.

C. Theoretical investigation of hydrogen passivation effects

We studied the effect of B doping with and without H incorporation on the electronic properties of BaSi$_2$. When a B atom is a substitutional impurity, degenerate p-type semiconducting properties occur regardless of the nonequivalent Si(3)–Si(5) positions (Fig. 1) occupied by a B atom. This happens because the Fermi level crosses some bands at the top of the valence band [Figs. 7(a)–7(c)]; this is because a B atom has three valence electrons while a Si atom has four, leading to a lower number of valence electrons in the system. As a consequence, this leads to a shift of the Fermi level to lower energies. However, if a H atom is directly bonded to a B atom at a substitutional site or bonded to any Si in the tetrahedron with a B atom, the Fermi level shifts to the gap, indicating that the semiconducting properties are no longer degenerate [Figs. 7(a′)–7(c′)], with no states in the gap region. Here, a H atom acts as a "donor" of one electron to a tetrahedron with a B atom, which provides almost the same DOS and is independent of the Si–H or B–H bonds.

In the case of a B atom acting as an interstitial impurity, we found three possible sites that differ in the number of first nearest neighbors to the B atom and their corresponding interatomic distances (see Fig. 8). For the first site, one partly occupied localized state and one filled localized state in the gap region are present in the corresponding DOS [Fig. 8(a)]. For the second site, one half-
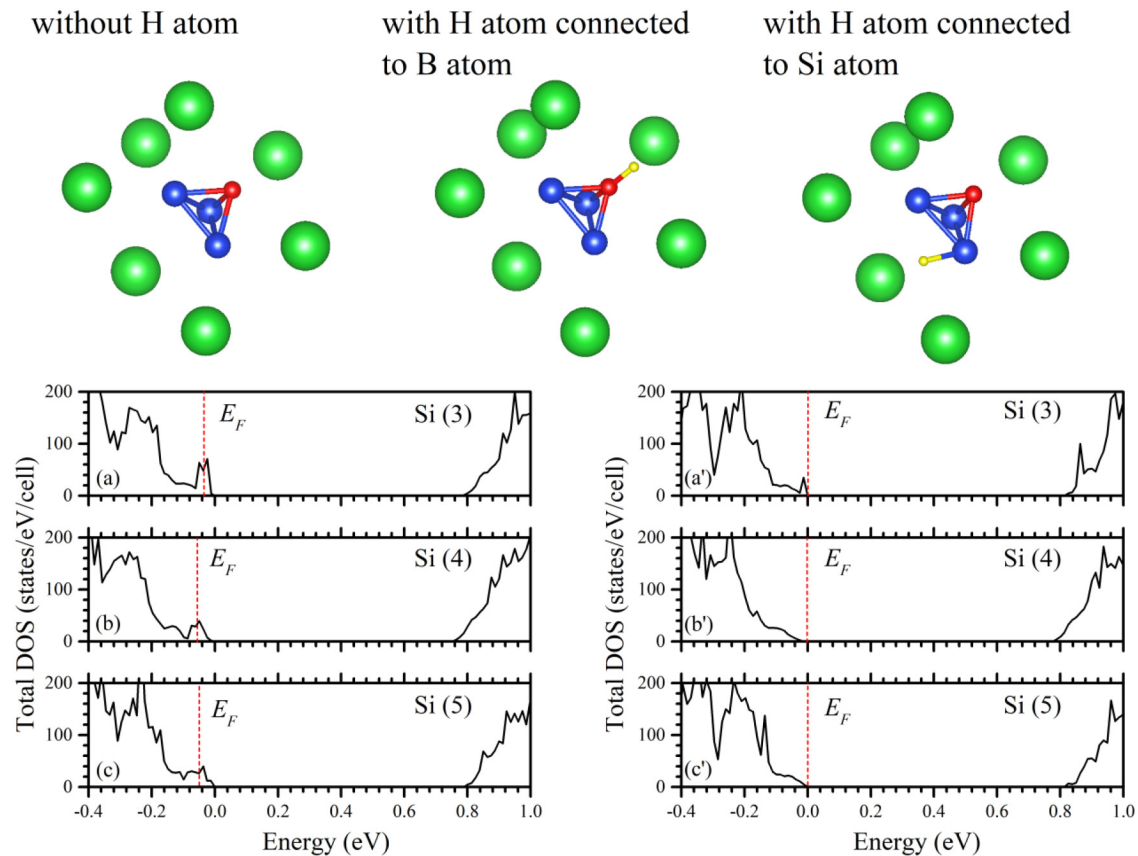
FIG. 7. Total density of states of BaSi$_2$ doped with B as a substitutional impurity in different Si [Si(3)–Si(5)] nonequivalent positions (a)–(c) without and (a′)–(c′) with H incorporation. Zero on the energy scale corresponds to the top of the valence band. The vertical dashed line indicates the Fermi level. Atomic configurations in the vicinity of the B atom are also shown. The large green spheres indicate Ba atoms, medium blue spheres stand for Si atoms, and B and H atoms are represented by small red and very small yellow spheres, respectively. The cases of Si–H and B–H bonding are shown in (a′) and (b′)–(c′), respectively.

filled localized state and one empty localized state can be observed in the gap region [Fig. 8(b)]. Finally, for the third site, degenerate n-type semiconducting properties occur [Fig. 8(c)]. When H is directly bonded to a B atom in any interstitial site, one filled localized state appears in the gap region [Figs. 8(a′)–8(c′)]. For the case of a substitutional impurity, when two H atoms are connected to a tetrahedron with a B atom, the localized state is clearly seen below the bottom of the conduction band [Fig. 9(a)]. For an interstitial impurity (two H atoms neighbor a B atom), the partly occupied localized state is evident in Figs. 9(b)–9(d). All the partly occupied states can serve as traps. It should be noted here that it is not necessary for all H atoms to be directly connected to an interstitial B atom. Like the case of a substitutional B impurity, H atoms can form bonds with Si atoms in a tetrahedron closest to the interstitial impurity without qualitative changes in the shape of the DOS with respect to the cases when only B–H bonds are present.

It is now possible to link the structural changes and electronic properties of our lightly doped samples. Thus, the structure of the sample fabricated with $t_{BaSi:H} = 0$ min (sample 1), which contains

states in the gap according to our photoresponse and PL measurements, can be characterized mainly by the cases represented in Figs. 8(a)–8(c) (i.e., by the presence of an interstitial B dopant), which also causes a relatively high trap concentration. As the concentration of incorporated H increases, the structure of the sample fabricated with $t_{BaSi:H} = 5$ min may be defined mainly by the cases represented in Figs. 8(a′)–8(c′). This, in turn, leads to a maximal "passivation" of B interstitials and a considerable decrease in the trap concentration because of the appearance of completely filled states that can no longer be viewed as traps. It should be noted that only one H atom is needed to reach this situation, in contrast to the presence of two H atoms for undoped BaSi$_2$.[27] Finally, when the H concentration is further increased, as for the sample fabricated with $t_{BaSi:H} = 10$ min (sample 3), the structure is characterized by the cases represented in Figs. 9(a)–9(d), where two H atoms increase the trap concentration. In addition, the incorporation of H itself in BaSi$_2$ also results in traps in the gap region.[27,34] Thus, H incorporation up to a certain concentration more efficiently neutralizes traps caused by B interstitials.
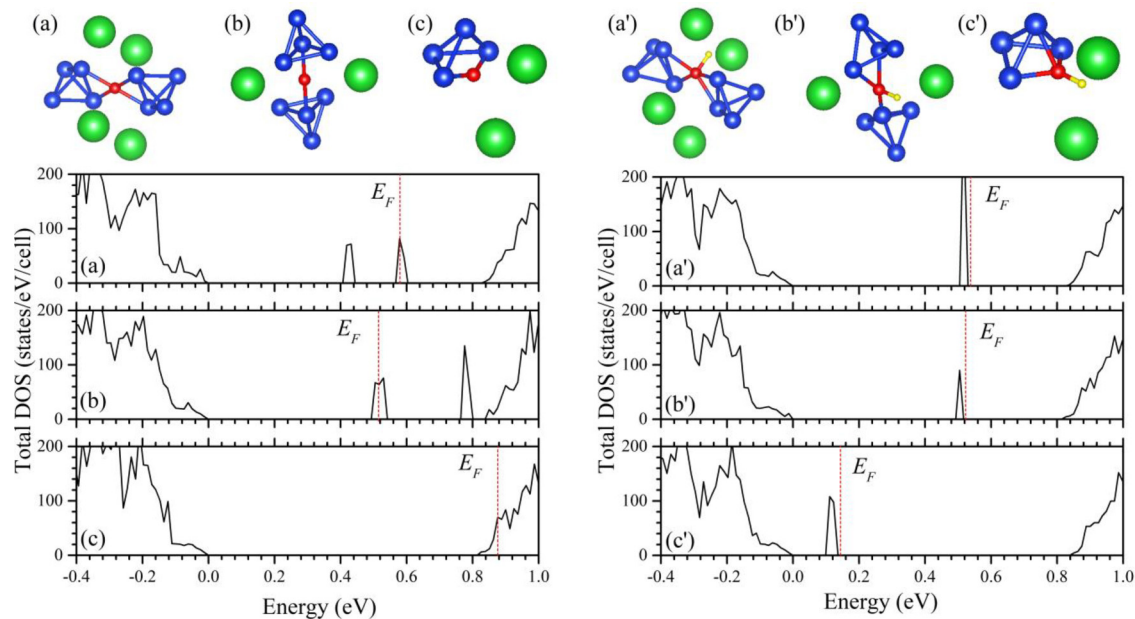
FIG. 8. Total density of states of (a)–(c) BaSi$_2$ doped with B as an interstitial impurity for three different cases depending on the number of first nearest neighbors and interatomic distances: (a) d_{Si-B} = 2.12–2.14 Å and d_{Ba-B} = 2.89–4.05 Å, (b) d_{Si-B} = 1.98 Å and d_{Ba-B} = 2.98 Å, and (c) d_{Si-B} = 1.89–2.21 Å and d_{Ba-B} = 3.05–3.19 Å. Total density of states of (a′)–(c′) are the same (a)–(c) cases but with one H atom bonded to the B atom. Zero on the energy scale corresponds to the top of the valence band. The vertical dashed line indicates the Fermi level. The corresponding atomic configurations in the vicinity of the B atom are also shown. The large green spheres indicate Ba atoms, medium blue spheres stand for Si atoms, and B and H atoms are represented by small red and very small yellow spheres, respectively.

For heavily B-doped BaSi$_2$ samples, the situation can be much more complex where, as we have indicated in Sec. III B, an increase in the neutral defect concentration (mainly interstitial B atoms) occurs. In the case of lightly B-doped BaSi$_2$ samples with a trap concentration of about 10^{14} cm^{-3}, our theoretical approach could reasonably well explain experimentally observed trends in photoresponsivity even though the minimal defect concentration in simulations could not be less than 10^{20} cm^{-3}. Therefore, to explain the experimentally observed trend of decreasing photoresponsivity with H incorporation in the heavily doped samples [see Fig. 2(b)], the other structural models are required involving the presence of a direct B–B bonding and/or two B atoms connected to the same Si tetrahedron. Surprisingly, a comparison of the total energy of cases with two interstitial B atoms directly bonded to each other [structural model in Fig. 10(a)] or to the same Si tetrahedron [structural model in Fig. 11(a)] indicated not only comparable values but even lower ones compared with the cases when two interstitial B atoms are far apart in the enlarged unit cell. Here, the excess B atoms lead to the formation of more complex defects: one B atom moves toward a neighboring Si tetrahedron and acts as a bridging atom between two Si atoms from different tetrahedra causing one Si–Si bond to be broken in the neighboring tetrahedron. An example of this defect is illustrated in Fig. 10(a), and the same is observed for the structural model in Fig. 11(a). As a result, a lot of states appear in the gap region according to the corresponding DOS [Figs. 10(a) and 11(a)]. One additional H atom increases the trap concentration

if two interstitial B atoms are directly bonded [Fig. 10(b)], regardless of Si–H or B–H bond formation, except for the case when the bridge configuration is broken by H atoms and n-type degenerate properties occur without states in the gap [Fig. 10(c)]. For the case of two interstitial B atoms connected to the same Si tetrahedron, one H atom is not capable of neutralizing multiple states in the gap [Figs. 11(b)–11(e)]. We have also checked the cases with one substitutional and one interstitial B atoms located in/at the same Si tetrahedron. In terms of formation energy, all such cases are energetically preferable with respect to the ones with two interstitial B atoms. In addition, the presence of B–B bonding is also found to be energetically favorable in any defect configuration. If two B atoms (one substitutional and one interstitial) are connected to each other (Fig. 12), no states are observed in the gap region [Fig. 12(a)]. Here, H incorporation provides a half-occupied state [Fig. 12(b)], except for the case when an H atom prevents formation of the bridge configuration [Fig. 12(c)]. If an interstitial B atom forms the Si–B bond with a Si atom in a tetrahedron with one substitutional B atom, the filled state appears in the gap, whereas H incorporation provides a half-occupied state (the Si–H bond or B–H bond with the interstitial B atom) similar to Fig. 12(b) or n-type degenerate properties (the B–H bond with the substitutional B atom) as in Fig. 12(c). To this end, the key issue of the heavily B-doped BaSi$_2$ samples is the appearance of the complex defect with two B atoms where in the most cases an addition of one H atom increases the trap concentration and, as a consequence,
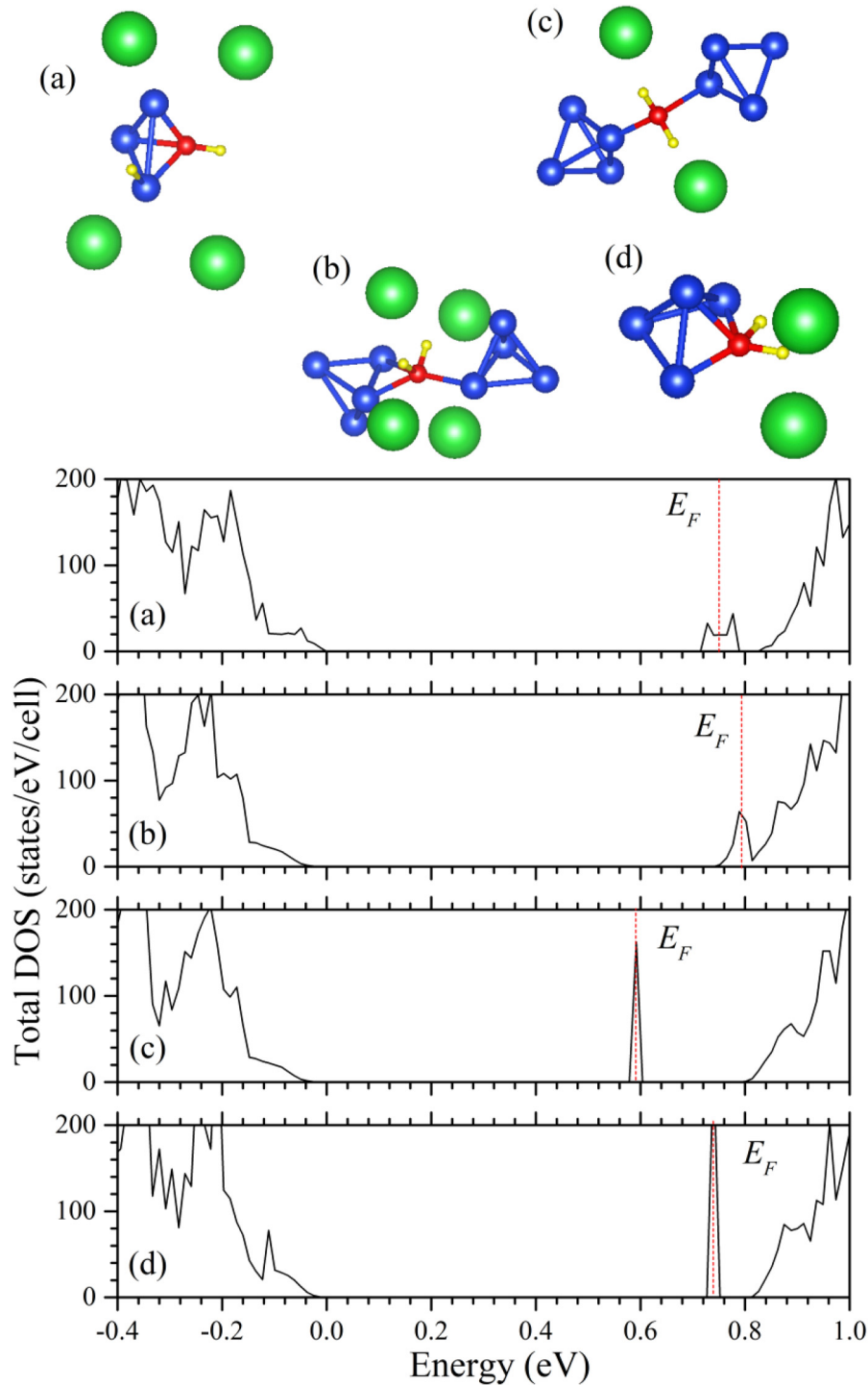
FIG. 9. Total density of states of BaSi$_2$ doped with B (a) as a substitutional impurity with two H atoms bonded to a tetrahedron with the B atom and (b)–(d) as an interstitial impurity with two H atoms bonded to the B atom. Zero on the energy scale corresponds to the top of the valence band. The vertical dashed line indicates the Fermi level. The corresponding atomic configurations in the vicinity of the B atom are also shown. The large green spheres indicate Ba atoms, medium blue spheres stand for Si atoms, and B and H atoms are represented by small red and very small yellow spheres, respectively.
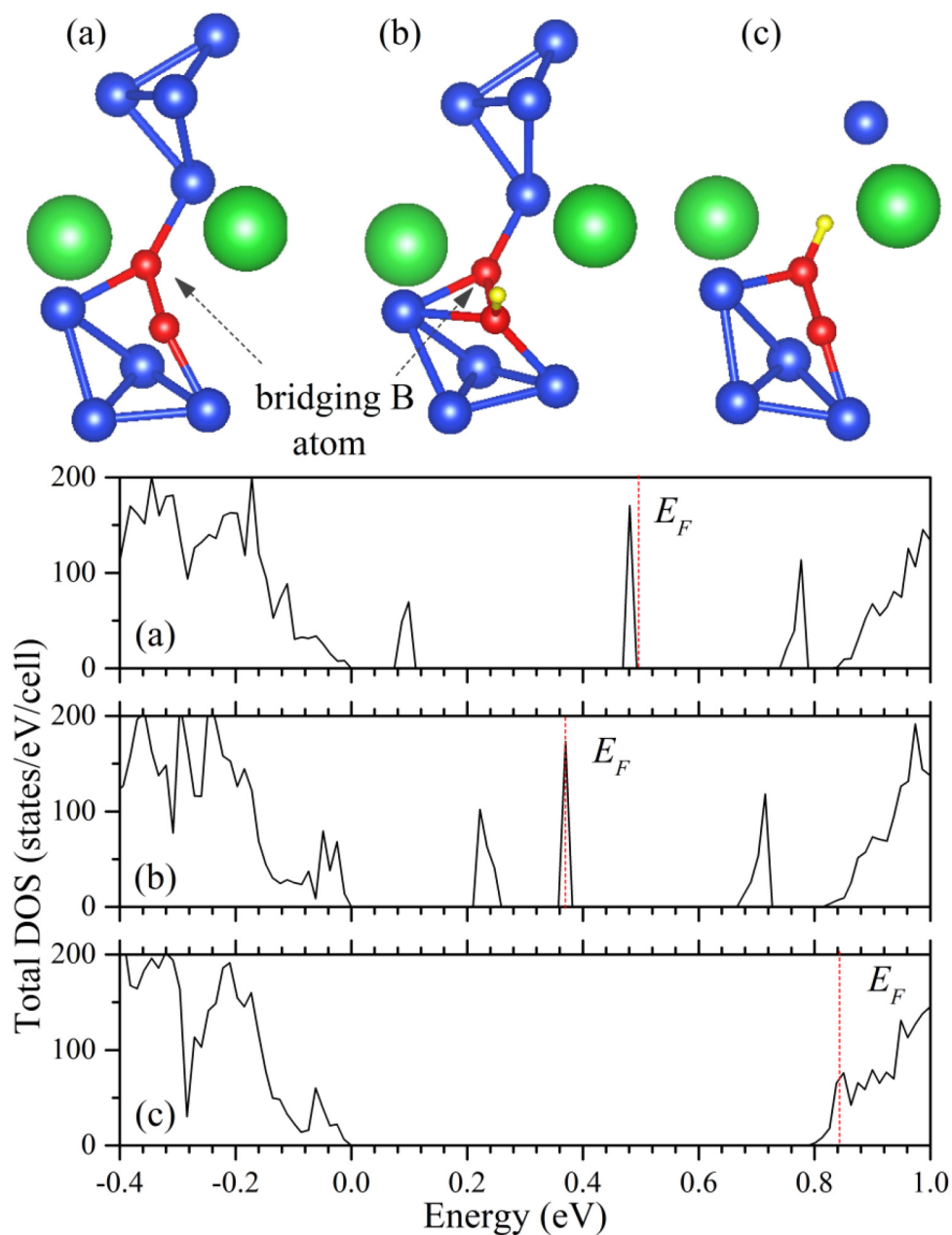
FIG. 10. Total density of states of BaSi$_2$ doped with two interstitial B connected to each other (a) without H passivation and (b)–(c) with H passivation. Zero on the energy scale corresponds to the top of the valence band. The vertical dashed line indicates the Fermi level. The corresponding atomic configurations in the vicinity of the B atom are also shown. The large green spheres indicate Ba atoms, medium blue spheres stand for Si atoms, and the B and H atoms are represented by small red and very small yellow spheres, respectively. The bridging B atoms are also indicated by arrows.

affects the photoresponsivity. We cannot exclude the possibility that a sizable amount of H atoms eventually neutralize these defects. However, considering that H atoms also act as interstitial defects,[27] such huge amount of H could worsen the situation.

In the enlarged unit cell used for calculations herein, only one type of defects can be treated at once because of serious limitations on the size of the considered systems. However, localized bands with very low dispersion appear in the energy gap region indicating
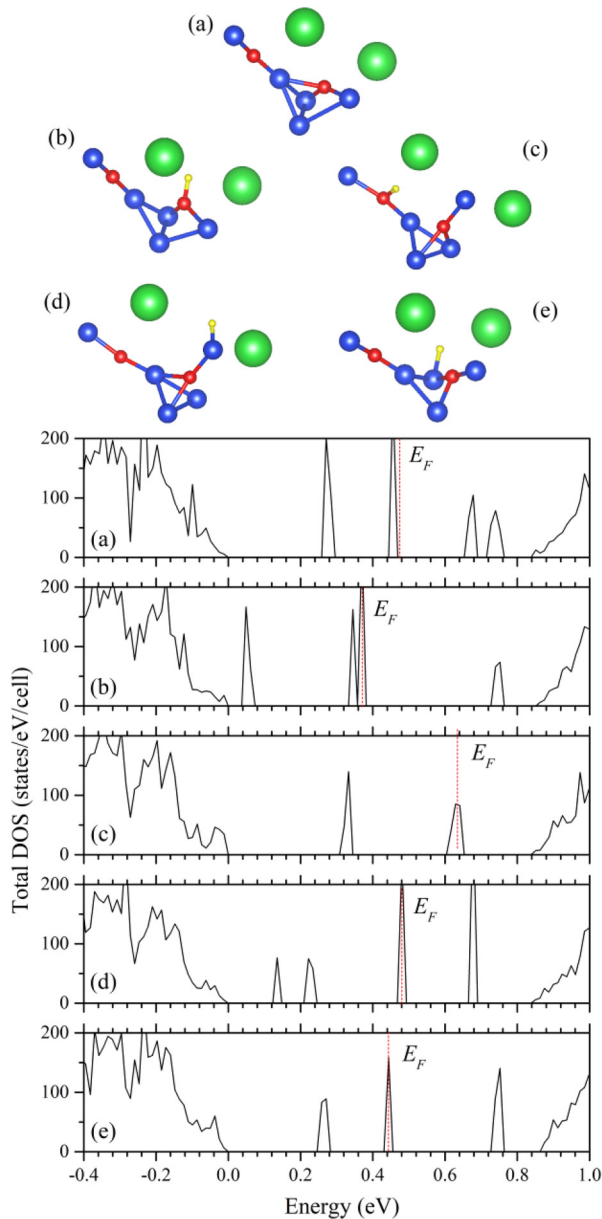
FIG. 11. Total density of states of BaSi$_2$ doped with two interstitial B connected to the Si tetrahedron (a) without H passivation and (b)–(e) with H passivation. Zero at the energy scale corresponds to the top of the valence band. The vertical dashed line indicates the Fermi level. The corresponding atomic configurations in the vicinity of the B atom are also shown. The large green spheres indicate Ba atoms, medium blue spheres stand for Si atoms, and the B and H atoms are represented by small red and very small yellow spheres, respectively.

that the defect–defect interaction is sizably attenuated. At the same time, in the direct space, everything is localized within the area of a defect. The latter fact in addition to the obtained n-type degenerate semiconducting properties [see Figs. 10(c) and 12(c)] does not

necessarily indicate a change in conductivity (from p-type to n-type) because in real B-doped BaSi$_2$ samples always various types of defects occur and the properties on the whole are defined by the defects with the largest concentrations. Since our heavily B-doped BaSi$_2$ samples do not show changes in the conductivity type (see Fig. 4), we can conclude that the defects responsible for n-type degenerate semiconducting properties do not dominate.

D. Effect of atomic H on the performance of p-BaSi$_2$/n-Si solar cells

Because heavily B-doped p-BaSi$_2$ films ($T_B = 1230\,°C$) were used in the p-BaSi$_2$/n-Si solar cells, we shortened the $t_{BaSi:H}$ from the optimum value for the lightly B-doped BaSi$_2$ films for the following reasons. As shown in Fig. 2(b) and the above discussions, the atomic H supply decreases the photoresponsivity of heavily B-doped p-BaSi$_2$ films. However, atomic H may passivate defects around the BaSi$_2$/Si interface from the result shown in Fig. 5(b). We, therefore, adopted $t_{BaSi:H}$ as 0, 14, and 30 s, as shown in Table II. Figure 13(a) shows the J–V curves of these solar cells under AM1.5 illumination. The short-current density (J_{SC}), open-circuit voltage (V_{OC}), fill factor (FF), and η all improved after atomic H passivation. To accurately determine the reverse saturation current density (J_0), the series resistance (R_S), and the shunt resistance (R_{SH}), we adopted a technique described by Sites and Mauk.[53] Using the photodiode equation, the relationship between R_S and R_{SH} can be given as

$$\frac{dV}{dJ} = SR_S + \frac{\gamma k_B T}{q}\left[\frac{1 - (SR_{SH})^{-1} - dV/dJ}{J + J_{SC} - (SR_{SH})^{-1}V}\right], \quad (1)$$

where S is the area of the electrode, γ is the ideality factor, k_B is the Boltzmann constant, T is the absolute temperature, and q is the elemental charge. The solar cell parameters obtained are summarized in Table III. The η improved from 2.59% in sample 11 ($t_{BaSi:H} = 0$ min) to a stable value of 6.20% in samples 12 and 13 ($t_{BaSi:H} = 14$ and 32 s, respectively), showing that η almost leveled off. Thus, further increasing $t_{BaSi:H}$ might degrade the solar cell performance. J_0 can be used as a measure to represent the quality of the p-BaSi$_2$/n-Si heterointerface, where a lower J_0 value indicates increased quality. The J_0 values of samples 12 and 13 were more than three orders of magnitude lower than that of sample 11. In other words, the defects around the heterointerface decreased markedly with H passivation. This result shows that even though no defect passivation is expected in the bulk region of the heavily B-doped BaSi$_2$ films on H treatment, improvements could be observed for the solar cell performance due to interface passivation. While the obtained η was not higher than the highest reported values, the effects of atomic H passivation were clearly demonstrated. Other factors, such as growth chamber conditions, that can degrade η require further investigation.

To investigate the defect densities and their levels in p-BaSi$_2$/n-Si solar cells, we performed DLTS measurements[54] on samples 11 and 12. Figure 13(b) shows a schematic diagram of the DLTS procedure, where a forward filling pulse voltage (V_P) disturbs the steady-state reverse-bias condition. This causes the electric field in the depletion region to decrease, thereby recharging the defect
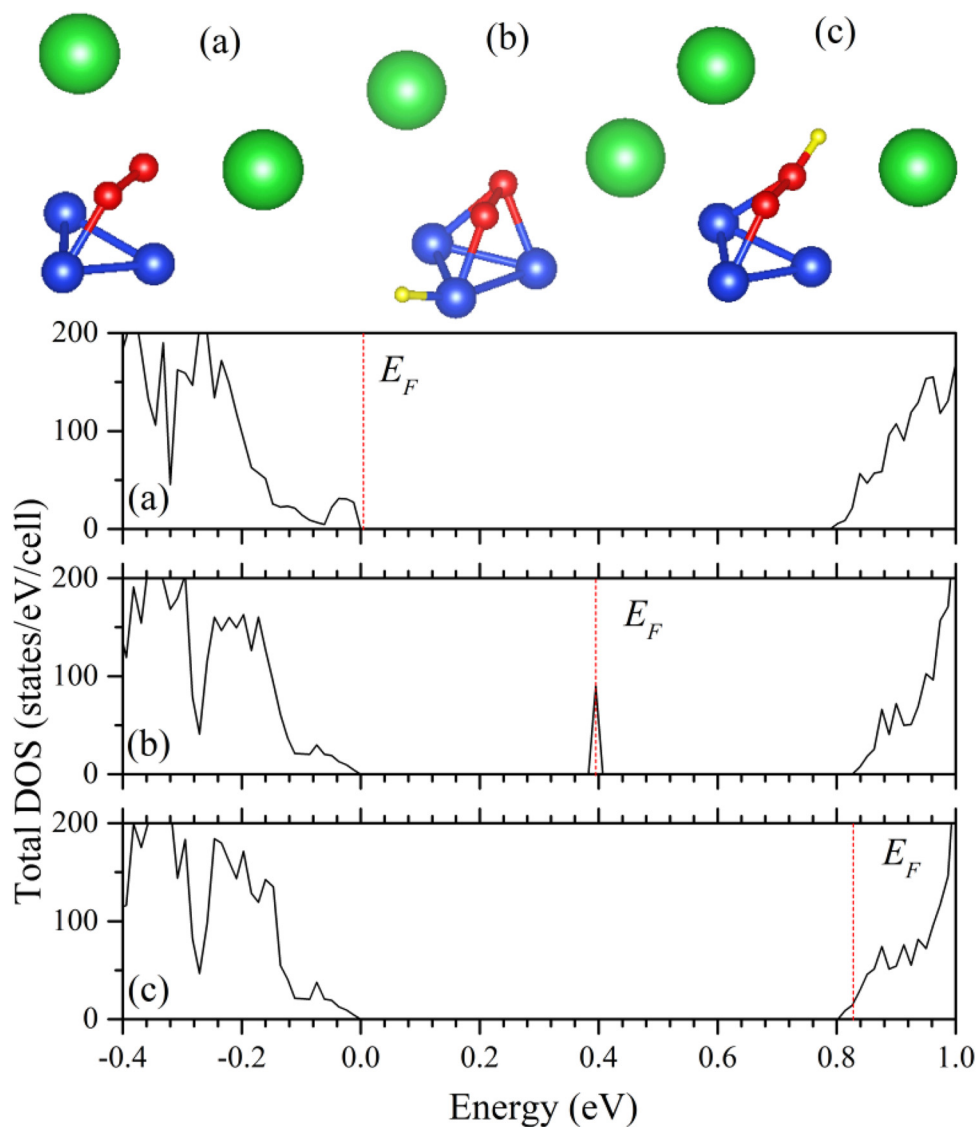
FIG. 12. Total density of states of BaSi$_2$ doped with two B substitutional and interstitial atoms connected to each other (a) without H passivation and (b)–(c) with H passivation. Zero on the energy scale corresponds to the top of the valence band. The vertical dashed line indicates the Fermi level. The corresponding atomic configurations in the vicinity of the B atom is also shown. The large green spheres indicate Ba atoms, medium blue spheres stand for Si atoms, and the B and H atoms are represented by small red and very small yellow spheres, respectively.

levels. When the voltage returns to its steady-state value, the defect levels begin to discharge by emitting trapped carriers by thermal emission, and the resultant time evolution of the capacitance change ΔC is measured for various rate windows. Here, V_P was set at 0.5 V, the pulse width (t_{PW}) at 50 ms, and the reverse bias voltage (V_R) at −0.1 V and −0.5 V. Because of a large difference in carrier concentration between p-BaSi$_2$ ($p > 10^{18}$ cm^{-3}) and n-Si ($n \approx 10^{15}$ cm^{-3}), the depletion region stretched toward the n-Si side. Therefore, defects in the n-Si side were detected. Figure 13(c) shows the DLTS profiles obtained for samples 11 and 12. A dip

caused by a majority carrier (electron) trap was observed at around 100 K in sample 11. On increasing the magnitude of V_R from 0.1 to 0.5 V, the signal intensity decreased. This indicates that the defects were present around the p-BaSi$_2$/n-Si interface. From the Arrhenius plot shown in Fig. 13(d), the electron trap level was calculated to be approximately 0.22 eV from the conduction band minimum, and the defect density was 1×10^{14} cm^{-3}. In contrast, no distinct peak was observed in sample 12, demonstrating that the defects in sample 11 were passivated by atomic H. The DLTS results are consistent with the improvement of the J–V curve
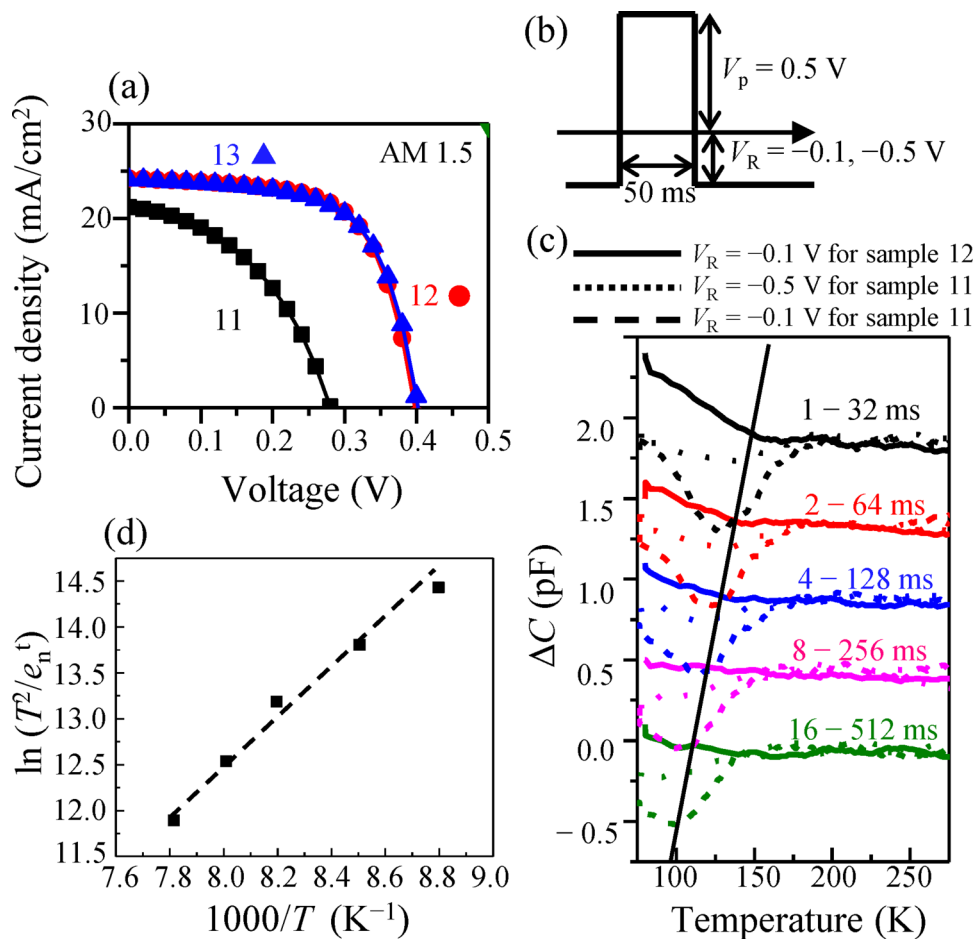
FIG. 13. (a) J–V characteristics of B-doped p-BaSi$_2$ ($p = 3 \times 10^{18}$ cm^{-3}, 20 nm)/n-Si solar cells with H passivation at different $t_{BaSi:H}$ under AM1.5 illumination (samples 11–13). (b) Schematic diagram of the DLTS procedure. (c) DLTS profiles of samples 11 and 12 at $V_p = 0.5$ V, $t_{pw} = 50$ ms, and $V_R = -0.1$ or -0.5 V. The rate window was varied as 1–32, 2–64, 4–128, 8–256, and 16–512 ms. (d) Arrhenius plot for the electron trap level.

shown in Fig. 13(a). Because of the significant reduction of interface defects, J_0 of samples 12 and 13 is approximately three orders of magnitude lower than that of sample 11. These DLTS results provide direct evidence that H irradiation is an effective means to improve solar cell performance by reducing interface defects. This discovery can be used in the near future to passivate interface defects in BaSi$_2$ homojunction solar cells.

TABLE III. Solar cell parameters of samples 11–13. Short-circuit current density (J_{SC}), open-circuit voltage (V_{OC}), fill factor (FF), conversion efficiency (η), series resistance (R_S), shunt resistance (R_{SH}), and reverse saturation current density (J_0) are all tabulated.

Sample	J_{SC} (mA/cm^2)	V_{OC} (V)	FF	η (%)	R_S (Ω)	R_{SH} (kΩ)	J_0 (mA/cm^2)
11	22	0.28	0.44	2.59	127	5.2	6.24×10^{-4}
12	27	0.40	0.63	6.20	92	22.3	4.42×10^{-7}
13	27	0.40	0.64	6.16	76	19.8	1.31×10^{-7}

IV. CONCLUSION

Our study clearly showed that in general the photoresponsivity of B-doped BaSi$_2$ can be significantly improved via H incorporation. An atomic H supply for $t_{BaSi:H} = 5$–10 min for lightly B-doped p-BaSi$_2$ films ($p = 7 \times 10^{16}$ cm^{-3} at RT) could enhance the photoresponsivity by up to an order of magnitude, while this was not the case for heavily B-doped p-BaSi$_2$ films ($p = 3 \times 10^{18}$ cm^{-3} at RT). The enhancement was caused by the increase in the minority-carrier lifetime, as measured by μ-PCD. However, further atomic H supply (≥ 15 min) led to significant degradation of photoresponsivity. An analysis of the experimental data shows that the overall photoresponsivity and the minority-carrier lifetime behavior could be explained in terms of various Auger processes. From the theoretical analysis, it could be concluded that (i) the trap concentration of lightly B-doped BaSi$_2$ is about one order higher ($\sim 10^{14}$ cm^{-3}) than that for the undoped BaSi$_2$ samples ($\sim 10^{13}$ cm^{-3}), which is in good agreement with the experimentally estimated value; (ii) the trap centers, should be associated with interstitial B atoms; (iii) for the lightly B-doped BaSi$_2$, a lower amount of hydrogen is needed to "passivate" these centers, compared with undoped BaSi$_2$; and (iv) the trap concentration of heavily B-doped BaSi$_2$ was in the order of 10^{15} cm^{-3} or even

higher, with interstitial B atoms tending to cluster. To understand this degradation, *ab initio* modeling was performed for various B-doped $BaSi_2$ structures with incorporated H atoms; the results indicated that a delicate balance exists between H as saturation species to eliminate trap states in the gap region originating from an interstitial B impurity and H as an interstitial impurity itself in $BaSi_2$ that leads to trap formation. We also investigated the effect of atomic H incorporation on the performance of B-doped p-$BaSi_2$/n-Si heterojunction solar cells, where an atomic H supply significantly decreased the reverse saturation current density and improved the conversion efficiency up to 6.2%. The reduction of defect density via atomic H supply was demonstrated via DLTS measurements.

DATA AVAILABILITY

The data that support the findings of this study are available from the corresponding author upon reasonable request.

REFERENCES

[1] J. Britt and C. Ferekides, Appl. Phys. Lett. **62**, 2851 (1993).
[2] A. Romeo, A. Terheggen, D. Abou-Ras, D. L. Bätzner, F. J. Haug, M. Kälin, D. Rudmann, and A. N. Tiwari, Prog. Photovoltaics **12**, 93 (2004).
[3] X. Wu, Sol. Energy **77**, 803 (2004).
[4] I. Repins, M. A. Contreras, B. Egaas, C. DeHart, J. Scharf, C. L. Perkins, B. To, and R. Noufi, Prog. Photovoltaics **16**, 235 (2008).
[5] H. Katagiri, K. Jimbo, W. S. Maw, K. Oishi, M. Yamazaki, H. Araki, and A. Takeuchi, Thin Solid Films **517**, 2455 (2009).
[6] P. Jackson, R. Wuerz, D. Hariskos, E. Lotter, W. Witte, and M. Powalla, Phys. Status Solidi Rapid Res. Lett. **10**, 583 (2016).
[7] H. L. Chen, A. Cattoni, R. D. Lépinau, A. W. Walker, O. Höhn, D. Lackner, G. Siefer, M. Faustini, N. Vandamme, J. Goffard, B. Behaghel, C. Dupuis, N. Bardou, F. Dimroth, and S. Collin, Nat. Energy **4**, 761 (2019).
[8] M. A. Green, A. Ho-Baillie, and H. J. Snaith, Nat. Photonics **8**, 506 (2014).
[9] W. S. Yang, J. H. Noh, N. J. Jeon, Y. C. Kim, S. Ryu, J. Seo, and S. I. Seok, Science **348**, 1234 (2015).
[10] T. Suemasu, Jpn. J. Appl. Phys. **54**, 07JA01 (2015).
[11] T. Suemasu and N. Usami, J. Phys. D Appl. Phys. **50**, 023001 (2017).
[12] K. Toh, T. Saito, and T. Suemasu, Jpn. J. Appl. Phys. **50**, 068001 (2011).
[13] D. B. Migas, V. L. Shaposhnikov, and V. E. Borisenko, Phys. Status Solidi B **244**, 2611 (2007).
[14] M. Kumar, N. Umezawa, and M. Imai, J. Appl. Phys. **115**, 203718 (2014).
[15] M. Kumar, N. Umezawa, and M. Imai, Appl. Phys. Express **7**, 071203 (2014).
[16] K. O. Hara, N. Usami, K. Nakamura, R. Takabe, M. Baba, K. Toko, and T. Suemasu, Appl. Phys. Express **6**, 112302 (2013).
[17] N. M. Shaalan, K. O. Hara, C. T. Trinh, Y. Nakagawa, and N. Usami, Mater. Sci. Semicon. Process. **76**, 37 (2018).
[18] M. Baba, M. Kohyama, and T. Suemasu, J. Appl. Phys. **120**, 085311 (2016).
[19] R. Takabe, S. Yachi, W. Du, D. Tsukahara, H. Takeuchi, K. Toko, and T. Suemasu, AIP Adv. **6**, 085107 (2016).
[20] T. Deng, T. Sato, Z. Xu, R. Takabe, S. Yachi, Y. Yamashita, K. Toko, and T. Suemasu, Appl. Phys. Express **11**, 062301 (2018).
[21] K. Kodama, Y. Yamashita, K. Toko, and T. Suemasu, Appl. Phys. Express **12**, 041005 (2019).
[22] M. Kumar, N. Umezawa, W. Zhou, and M. Imai, J. Mater. Chem. A **5**, 25293 (2017).
[23] Y. Yamashita, T. Sato, Miftahullatif Emha Bayu, K. Toko, and T. Suemasu, Jpn. J. Appl. Phys. **57**, 075801 (2018).
[24] T. Sato, H. Hoshida, R. Takabe, K. Toko, Y. Terai, and T. Suemasu, J. Appl. Phys. **124**, 025301 (2018).
[25] T. Sato, C. Lombard, Y. Yamashita, Z. Xu, L. Benincasa, K. Toko, S. Gambarelli, and T. Suemasu, Appl. Phys. Express **12**, 061005 (2019).
[26] T. Sato, Y. Yamashita, Z. Xu, K. Toko, S. Gambarelli, M. Imai, and T. Suemasu, Appl. Phys. Express **12**, 111001 (2019).
[27] Z. Xu, D. A. Shohonov, A. B. Filonov, K. Gotoh, T. Deng, S. Honda, K. Toko, N. Usami, D. B. Migas, V. E. Borisenko, and T. Suemasu, Phys. Rev. Mater. **3**, 065403 (2019).
[28] S. Sugiyama, Y. Yamashita, K. Toko, and T. Suemasu, Jpn. J. Appl. Phys. **59**, SFFA04 (2020).
[29] G. Kresse and J. Hafner, Phys. Rev. B **49**, 14251 (1994).
[30] G. Kresse and J. Furthmüller, Phys. Rev. B **54**, 11169 (1996).
[31] G. Kresse and J. Joubert, Phys. Rev. B **59**, 1758 (1999).
[32] J. Evers, J. Solid State Chem. **32**, 77 (1980).
[33] D. A. Shohonov, D. B. Migas, A. B. Filonov, V. E. Borisenko, R. Takabe, and T. Suemasu, Thin Solid Films **686**, 137436 (2019).
[34] Z. Xu, T. Sato, J. Nakamura, A. Koda, K. Shimomura, A. B. Filonov, D. B. Migas, and T. Suemasu, Jpn. J. Appl. Phys. (in press).
[35] J. P. Perdew, S. Burke, and M. Ernzerhof, Phys. Rev. Lett. **77**, 3865 (1996).
[36] S. M. Sze, *Physics of Semiconductor Devices*, 2nd ed. (Wiley, New York, 1981).
[37] D. Chen, P. G. Hamer, M. Kim, T. H. Fung, G. Bourret-Sicotte, S. Liu, G. E. Chan, A. Ciesla, R. Chen, M. D. Abbott, B. J. Hallam, and S. R. Wenham, Sol. Energy Mater. Sol. C **185**, 174 (2018).
[38] M. Tajima, J. Cryst. Growth **103**, 1 (1990).
[39] E. C. Lightowlers and V. Higgs, Phys. Status Solidi A **138**, 665 (1993).
[40] M. Tajima, Y. Iwata, F. Okayama, H. Toyota, H. Onodera, and T. Sekiguchi, J. Appl. Phys. **111**, 113523 (2012).
[41] S. Shirakata and T. Nakada, Thin Solid Films **515**, 6151 (2007).
[42] J. K. Larsen, S. Y. Li, J. J. S. Scragg, Y. Ren, C. Hägglund, M. D. Heinemann, S. Kretzshmar, T. Unold, and C. Platzer-Björkman, J. Appl. Phys. **118**, 035307 (2015).
[43] P. M. P. Salome, J. P. Teixeira, J. Keller, T. Torndahl, S. Sadewasser, and J. P. Leitao, IEEE J. Photovoltaics **7**, 670 (2017).
[44] A. Le Bris, L. Lombez, S. Laribi, G. Boissier, P. Christol, and J. F. Guillemoles, Energy Environ. Sci. **5**, 6225 (2012).
[45] J. K. Katahara and H. W. Hillhouse, J. Appl. Phys. **116**, 173504 (2014).
[46] T. Okamoto, Y. Matsuzaki, N. Amin, A. Yamada, and M. Konagai, Jpn. J. Appl. Phys. **37**, 3894 (1998).
[47] D. P. Halliday, J. M. Eggleston, and K. Durose, J. Cryst. Growth **186**, 543 (1998).
[48] I. L. Braly, D. W. deQilettes, L. M. Pazos-Qutón, S. Burke, M. E. Ziffer, D. S. Ginger, and H. W. Hillhouse, Nat. Photonics **12**, 355 (2018).
[49] W. Shockley and W. T. Read, Jr., Phys. Rev. **87**, 835 (1952).
[50] J. I. Pankove, D. E. Carlson, J. E. Berkeyheiser, and R. O. Wance, Phys. Rev. Lett. **51**, 2224 (1983).
[51] N. M. Johnson, C. Herring, and D. J. Chadi, Phys. Rev. Lett. **56**, 769 (1986).
[52] T. Deng, T. Suemasu, D. A. Shohonov, I. S. Samusevich, A. B. Filonov, D. B. Migas, and V. E. Borisenko, Thin Solid Films **661**, 7 (2018).
[53] J. R. Sites and P. H. Mauk, Sol. Cells **27**, 411 (1989).
[54] D. V. Lang, J. Appl. Phys. **45**, 3023 (1974).